Sintering properties of sol–gel derived lithium disilicate glass ceramics

Feng Wang[1,2] . Ke Li[1] . Congqin Ning[1]

1. State Key Laboratory of High Performance Ceramics and Superfine Microstructure, Shanghai Institute of Ceramics, Chinese Academy of Sciences, Shanghai 200050, China
2. NTNU Nanomechanical Lab, Department of Structural Engineering, Norwegian University of Science and Technology (NTNU), Trondheim 7491, Norway
*Email:cqning@mail.sic.ac.cn

Abstract

Lithium disilicate (Li2Si2O5) glass-ceramics were fabricated through two sol–gel methods: the nitrate route and the alkoxide route. Thermal analysis revealed different crystallization processing of two gel-derived powders. Li2Si2O5 powders were obtained after heat treatment at 800 °C. These powders were pressed and pressureless sintered under 900–1030 °C. Microstructure of sintered samples revealed the grain size and morphology of Li2Si2O5 ceramics. Although grain size in both samples increased with increasing sintering temperature, samples from the alkoxide route derived powders had more uniform grain size and pore distribution. In addition, open porosity decreased in both samples with increasing sintering temperature. Unlike familiar nucleation that resulted in grain growth mechanism, the Li2Si2O5 particles developed into irregular large size grains at first, and then grew into rod-shaped grains.

Graphical Abstract

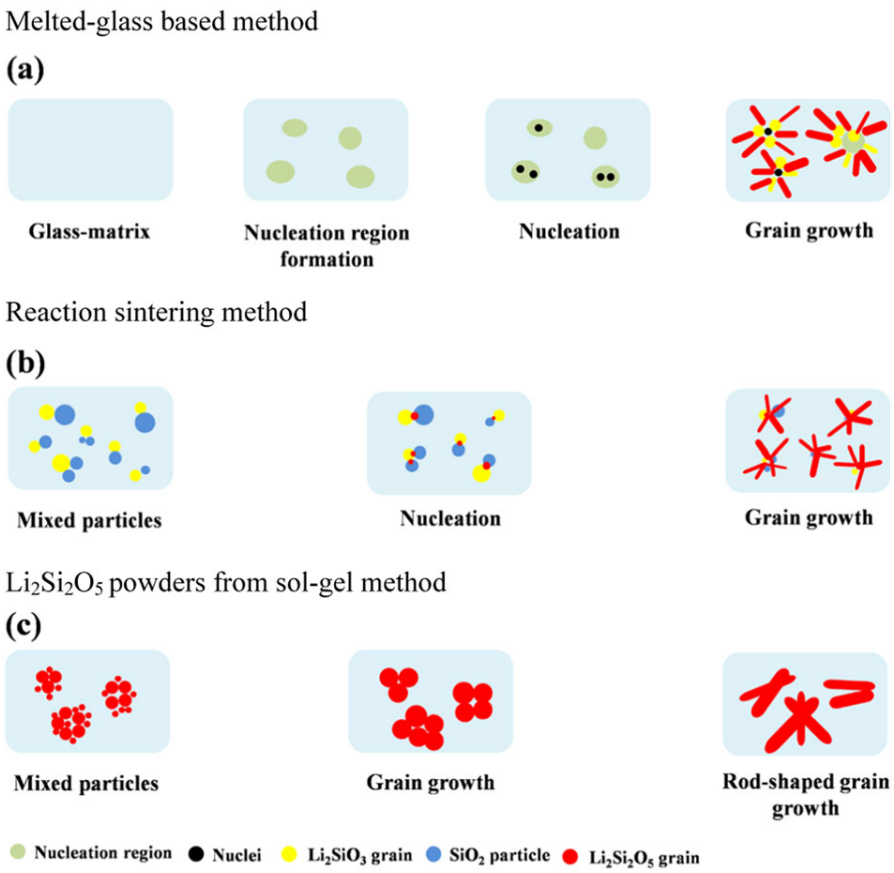

Highlights

- Lithium disilicate glass-ceramics were fabricated through two sol-gel methods;
- New grain growth mechanism of rodlike $Li_2Si_2O_5$ grains was illustrated;
- Sintering property of sol-gel derived $Li_2Si_2O_5$ is more like that of ceramics.

Keywords Sol-gel, Lithium disilicate, Glass-ceramics, Pressureless sintering.

1. Introduction

In the last decades, all-ceramic materials have been widely used for fixed restoration in dentistry because of their great esthetic appearance [1-7]. In these materials, lithium disilicate ($Li_2Si_2O_5$) glass-ceramics that possess both high strength and distinctive translucency characteristics have aroused increasing attention [8-13].

Generally, lithium disilicate glass-ceramics can be fabricated through various methods[14] such as melting-casting-crystallization[19-21], sol-gel[14-17], sintering of glass frits[22-25], and reaction sintering[26]. For melting-casting-crystallization method, the oxides with low melting point (like ZnO、CaO、K_2O、B_2O_3, etc) are always used to reduce the melting temperature of Li_2O–SiO_2 system.[20, 23, 28]. However the melting temperature was still high to 1300-1400℃. For powder sintering method, Li_2O–SiO_2 binary glass systems also need to be melted around 1300-1550℃[25, 29, 30]. Comparing with these methods above, sol-gel method can obtain lithium disilicate glass-ceramics from precursors of Li_2O and SiO_2 without high temperature melting procedure. Lithium disilicate could be fabricated directly after heat-treating at 500-900℃.

In sol-gel method, tetraethylorthosilicate (TEOS) is most often used as silicon source, the precursor of lithium can be varied from alkoxides (such as lithium methoxide and lithium ethoxide) to inorganics (such as $LiNO_3$ and LiOH). Li et al.[28] fabricated $Li_2Si_2O_5$ through sol-gel method from various lithium precursors and explained how crystalline phase development in these gel-derived powders. In sol-gel method, crystalline phase of $Li_2Si_2O_5$ can be obtained after a treatment at 550-600℃. Coupled with this study, lithium disilicate glass-ceramics have been successfully fabricated by controlling crystallization behaviors in sol-gel methods[17,18]. However, few research focused on sintering properties of sol-gel derived $Li_2Si_2O_5$ glass-ceramic powders.

In the present study, $Li_2Si_2O_5$ glass-ceramic powders were fabricated through two sol-gel methods, and the sintering behavior of two powders were investigated and contrasted. $Li_2Si_2O_5$ glass-ceramic powders were pressed into blocks and subsequently pressureless sintered under various temperatures. Microstructures of sintered bodies were detected and sintering characteristics of these powders were discussed.

2. Experimental Procedure

2.1. Sol-gel preparation of $Li_2Si_2O_5$ glass-ceramic powders

Two solution routes were utilized in this study: (1) $LiNO_3$ (AR, Shanghai Fengshun Chemical Technology Co., Ltd, China) combined with TEOS (AR, Shanghai Lingfeng Chemical Reagent Co., Ltd, China); (2) $LiOC_2H_5$ combined with TEOS.

For the nitrate route, $LiNO_3$ was first dissolved in distilled water and then added to TEOS with ethanol added to permit miscibility (n(TEOS):n(H_2O):n(ethanol)=1:8:4, with Si/Li molar ratio of 1/1 according to the molecular formula of lithium disilicate). The mixture was mechanicallly

stirred under a rotate speed of 300r/min at room temperature (~25℃) until complete hydrolysis (a translation from initial immiscible solutions to a homogenous and clear solution can be observed when hydrolysis complete). The solution was aged at 60℃ for 12h to obtain clear gel. The gel was dried at 120℃ and ground to powder using an agate mortar and pestle.

For the alkoxide route, TEOS and lithium (3N, Sinopharm Chemical Reagent Co., Ltd, China) were dissolved into ethanol to obtain ethanolic solutions of TEOS (2mol/L) and lithium ethoxide ($LiOC_2H_5$, 0.82mol/L), respectively. Then the sol was prepared at room temperature (~25℃) by mixing ethanolic solutions of TEOS and $LiOC_2H_5$ with a Si/Li molar ratio of 1/1 according to the molecular formula of lithium disilicate. The above TEOS/$LiOC_2H_5$ mixture was mechanically stirred for 3 hours with a rotate speed of 300r/min. A proper amount of water/ethanol mixture with an ethanol/water ratio of 2/1 (in volume) was then added into the TEOS/$LiOC_2H_5$ solution. The gelation was completed in ten seconds. After being kept at 60℃ for 12h, the gel was dried at 90℃ and then ground to powders.

Dried gel-derived powders were heat-treated at 600℃for1h with a heating rate of 3℃/min, then calcined at 800℃ for 2h with a heating rate of 2℃/min in air atmosphere to obtain $Li_2Si_2O_5$ glass-ceramic powders. The calcined powders were ground and then sieved through a 200-mesh screen for the following study.

2.2. Sintering of sol-gel derived $Li_2Si_2O_5$ glass-ceramic powders

The calcined $Li_2Si_2O_5$ powders were pressed into blocks with dimensions of 5.0mm×6.0mm×50.0mm under 12MPa, followed by a cold isostatic pressing at 280MPa. These samples were sintered pressurelessly at 950-1030℃ for 2h in air atmosphere with a heating rate of 3℃/min. The samples sintered from powders fabricated through nitrate route and alkoxide route were named as NR and AR, respectively. NR950-NR1030 and AR950-AR1030 represented samples sintered at temperature from 950-1030℃.

2.3. Characterization

The organic decomposition and crystallization behavior of gel-derived powders were analyzed by thermos gravimetric analysis (TGA) and differential thermal analysis (DTA) on a simultaneous thermal analysis (STA) instrument (Thermoplus EVOII, Rigaku, Japan) with a heating rate of 10℃ /min and an air flow of 30 ml/min. The mass of the samples used was 13mg for both powders. Crystalline phases of the heat-treated powders were identified by X-ray diffractometry (XRD, D/MAX-RBX, Rigaku, Osaka, Japan) with Cu Kα radiation (λ=0.15418 nm). Open porosity of the sintered samples was determined by the Archimedes method using distilled water as medium. Morphologies of the heat-treated powders and the sintered samples were observed by scanning electron microscopy (SEM, S-4800N, Hitachi, Japan). To get a clear grain morphology, the as-sintered sample surface was etched by 2vol.% HF solution for 120s.

3. Results and Discussion

3.1. TGA/DTA Analyses

Thermal analysis data of sol-gel derived powders from nitrate route and alkoxide route are shown in Fig. 1. Powders were dried at 120℃ before analysis. It should be noticed that weight loss

reached equilibrium at around 630℃ in Fig. 1(a) and 500℃in Fig. 1(b), which meant the gels were complete decomposed. Thus, the thermal changes upper than the temperatures should belong to crystallization of lithium silicate phases. For the nitrate route (Fig. 1a), weight loss below 110℃ combined with an endotherm peak was attributed to the removal of physical bound water. This endotherm peak was not supposed to happen for dry powders. Thus, the extra water might cause by nitrates, the hygroscopicity of nitrides may catch some water vapor from air during the procedure when transfer powders from oven to the STA instrument. The second endotherm peak at 258℃ can be assigned to the melting of $LiNO_3$. In the TGA curve, the gradual weight loss from 110 to 520℃was due to organic decomposition. At the same time, in this temperature range, the slowly heat change started around ~ 400 ℃ with small weight loss was related to the reaction between nitrates and silica through equation (2) and Li_2SiO_3 formed, which coincided with XRD results of P. Li *et al* [31]. The progress of this reaction was slow, thus heat flow changed slowly without obvious peaks appeared. The weight loss through gas leaking was also unapparent. As temperature increasing, a rapid weight loss from 520℃ to 630℃ in TGA curve and a broad endothermic peak at ~590℃in DTA curve were observed. This was caused by the intense decomposition of nitrates at higher temperature through equation (1), which resulted in a rapid crystallization of lithium silicate phases (Li_2SiO_3, $Li_2Si_2O_5$) through equations (4) and (6). Reaction through equations (2), (3) and (5) would exist simultaneously. This temperature range was the main section for $Li_2Si_2O_5$ crystallization. Powders from alkoxide route showed a total different TGA-DTA curve in Fig. 1(b) comparing with nitrate-derived powders. Removal of physically bound volatiles occurred at 170℃ with an endotherm in the DTA curve and weight loss in the TGA data. The sustained weight loss from 170 to 500℃ in TGA was due to the decomposition of residual organic produced from hydrolysis/condensation reactions. An exothermic peak occurred at ~581℃, which should correspond to the crystallization of lithium silicate phases (Li_2SiO_3, $Li_2Si_2O_5$) [17]. No Li_2SiO_3 was detected in the following XRD pattern of powders from alkoxide route. Because a transfer from Li_2SiO_3 to $Li_2Si_2O_5$ occurred at higher temperature, which was similar to the results of Bo et al[17]. After crystallization of the lithium silicate phases, the weight loss of the alkoxide route was lower than the nitrate route. More lithium silicate crystal phases existed in the samples from the alkoxide route. Thus the heat flow resulted from the growth of crystals had higher tail covers around 100 microvolts in Fig. 1(b) than 15 microvolts in Fig. 1(a).

$$2LiNO_3 \rightarrow Li_2O + 2NO_2(g) + \frac{1}{2}O_2(g) \quad (1)$$

$$2LiNO_3 + SiO_2 \rightarrow Li_2SiO_3 + 2NO_2(g) + \frac{1}{2}O_2(g) \quad (2)$$

$$2LiNO_3 + 2SiO_2 \rightarrow Li_2Si_2O_5 + 2NO_2(g) + \frac{1}{2}O_2(g) \quad (3)$$

$$Li_2O + SiO_2 \rightarrow Li_2SiO_3 \quad (4)$$

$$Li_2SiO_3 + SiO_2 \rightarrow Li_2Si_2O_5 \quad (5)$$

$$Li_2O + 2SiO_2 \rightarrow Li_2Si_2O_5 \quad (6)$$

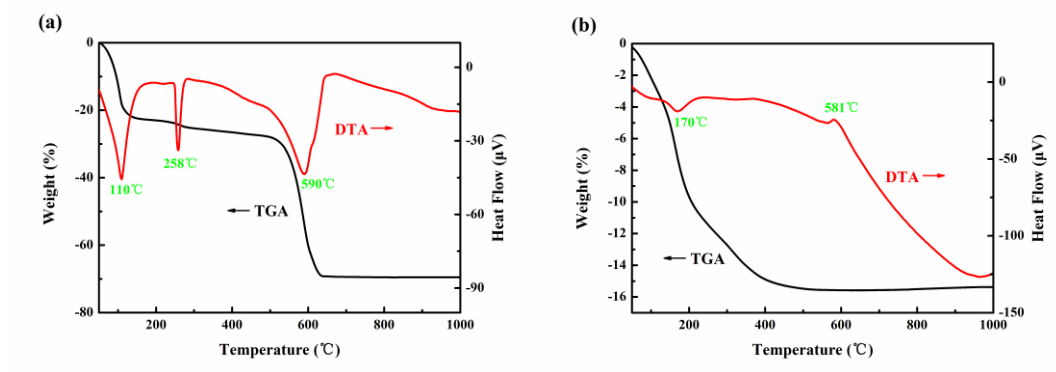

Fig. 1 TGA/DTA data for gel-derived powders prepared by: (a) the nitrate route; (b) the alkoxide route.

3.2. Characterization of the Calcined Powders

After calcination treatment at 800℃, lithium silicate powders were obtained. Fig. 2 showed the SEM and optical photographs of as-prepared $Li_2Si_2O_5$ powders through two different routes. The $Li_2Si_2O_5$ powders fabricated through the nitrate route showed a white appearance after heat treatment, while the powders from alkoxide route were gray in color, which might be attributed to the residual carbon produced during the decomposition of alkoxide in this method [17]. Since the carbon were tapped in very small pores in the gel, it was hard to be eliminated. Because small carbon amount changes was hard to be accuracy measured by the machine used, no further weight loss were detected in the TGA/DTA data for powders from alkoxide route after 500℃. The residual carbon may located at the grain boundaries of $Li_2Si_2O_5$ and lower the mass transfer efficiency of the grains and affected both grain growth in crystallization and densification in sintering procedure. Compared the SEM images in Fig .2, we could see that $Li_2Si_2O_5$ powders prepared by alkoxide route were much more homogenous than the powders prepared by nitrate route, and the former one had much smaller particle size. As the heating procedures were the same, the differences between particles size were resulted from solutions and gelling processings. One possible reason was that less water were used in the alkoxide route, the hydrolysis ratio was lower and resulted in smaller initial particle-sites.

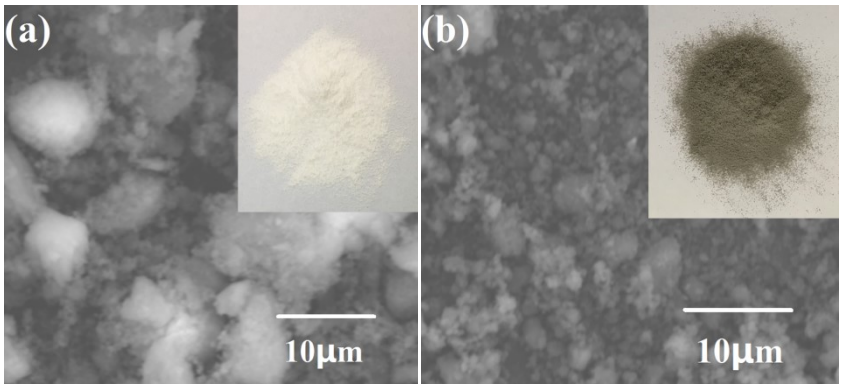

Fig. 2 SEM and optical photographs of calcined $Li_2Si_2O_5$ powders prepared by: (a) the nitrate route; (b) the alkoxide route.

XRD patterns of the calcined powders at 800℃ were shown in Fig. 3. It should be noted that $Li_2Si_2O_5$ is the main phase of both powders (PDF#72-0102). However, diffraction peaks of Li_2SiO_3 were also detected in the powders prepared by nitrate route, which coincided with the previous reference[31]. It has been proved that metastable Li_2SiO_3 crystallized firstly at ~450℃ prior to the crystallization of $Li_2Si_2O_5$ phase when $LiNO_3$ was used as lithium source. The decomposition of nitrates might be beneficial to the crystallization of Li_2SiO_3. At the higher temperature, Li_2SiO_3 might transform to $Li_2Si_2O_5$ phase through a further reaction with SiO_2. In general, gel structure, $LiNO_3$ crystallite size and distribution in the gel, and the hydrolysis ratio would affect the phase composition in the powders prepared by nitride route. On the contrary, $Li_2Si_2O_5$ was the only phase of the powders prepared by alkoxide route.

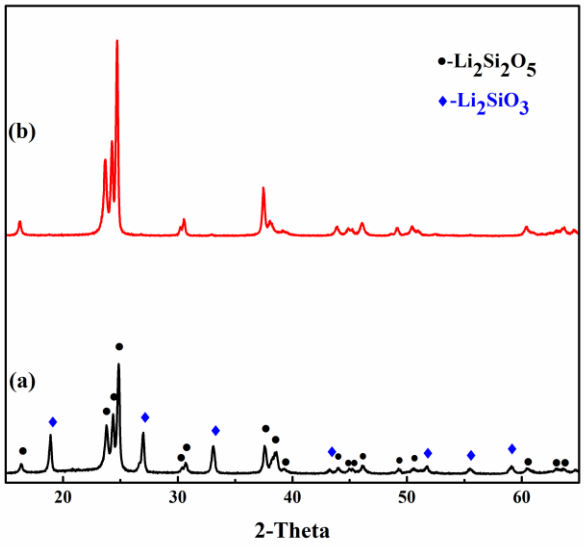

Fig. 3 XRD patterns of as-calcined $Li_2Si_2O_5$ powders at 800℃ prepared by nitrate route (a) and alkoxide route (b).

3.3. Microstructure and Open Porosity of Sintered Samples

Fig. 4 showed the SEM micrographs of the fracture surface of sintered samples at various temperatures. Apparently, for both NR and AR cases, the grain size increased with increasing sintering temperature from 950℃ to 1030℃. The volume diffusion through the necks between lithium silicate grains resulted in increasing in density, which was proved by Fig. 5. Fig. 4(e) and Fig. 4(f) showed a much larger grain size and no obviously grain boundaries were observed when sintering temperature increased to 1030 ℃, indicating liquid sintering occurred at higher temperatures. As shown by the low-magnification images in Fig. 4(a) and Fig. 4(b), AR950 had more homogenous microstructure comparing with NR950, which was attributed to the uniform particle distribution and good dispersibility of $Li_2Si_2O_5$ powders from alkoxide route. Generally, aggregated particles were easily to be sintered together and grew into large grains, so the extraordinarily large grains in Fig. 4(e) were developed from the aggregated particles in nitrate-route powders. The pore distribution was also uniform in AR1030 as what was shown in Fig. 4(e) and Fig. 4(f). Open porosity of the sintered bulks was measured as shown in Fig. 5, the porosity decreased as sintering temperature increasing. The porosity decreased faster as the sintering

temperature increased to higher than 1010℃, which was in accordance with the SEM figures. The grain size increased greatly in AR1030 and NR1030, which can significantly promote pores elimination. As mentioned above, powders fabricated from nitrate route possessed poor dispersibility, and the aggregated particles were easy to be sintered together at the beginning of sintering procedure. This might be the main reason why NR950-1010 showed a lower open porosity comparing with AR950-1010, which was in accordance with the micrographs shown in Fig. 4. However, as sintering temperature increasing, pores among uniform stacked particles were easier to be exhausted. Consequently, open porosity in AR1030 was lower than NR1030.

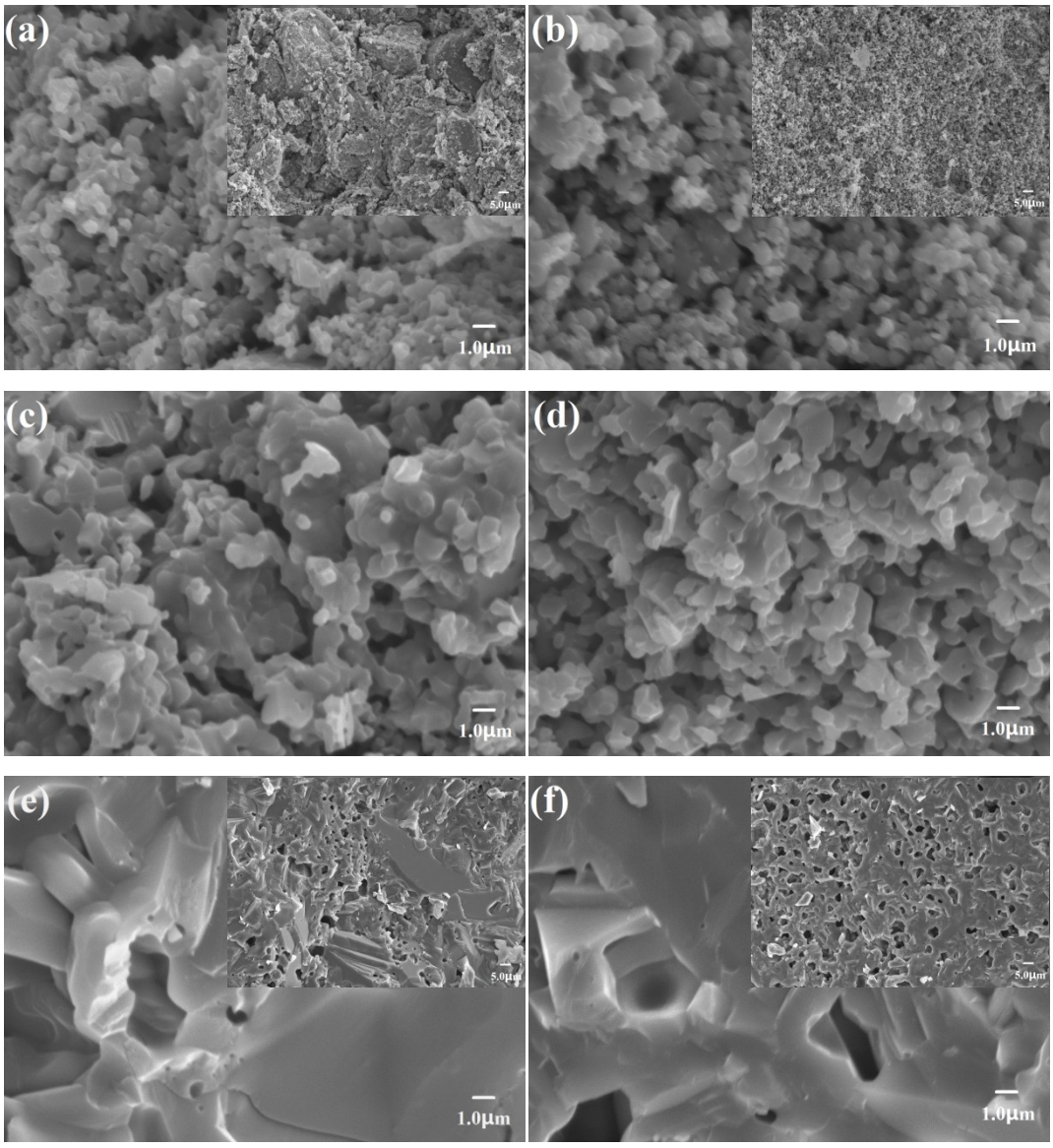

Fig. 4 SEM micrographs of the fracture surface of sintered samples: (a) NR950; (b) AR950; (c) NR990; (d) AR990;(e) NR1030; (f) AR1030;

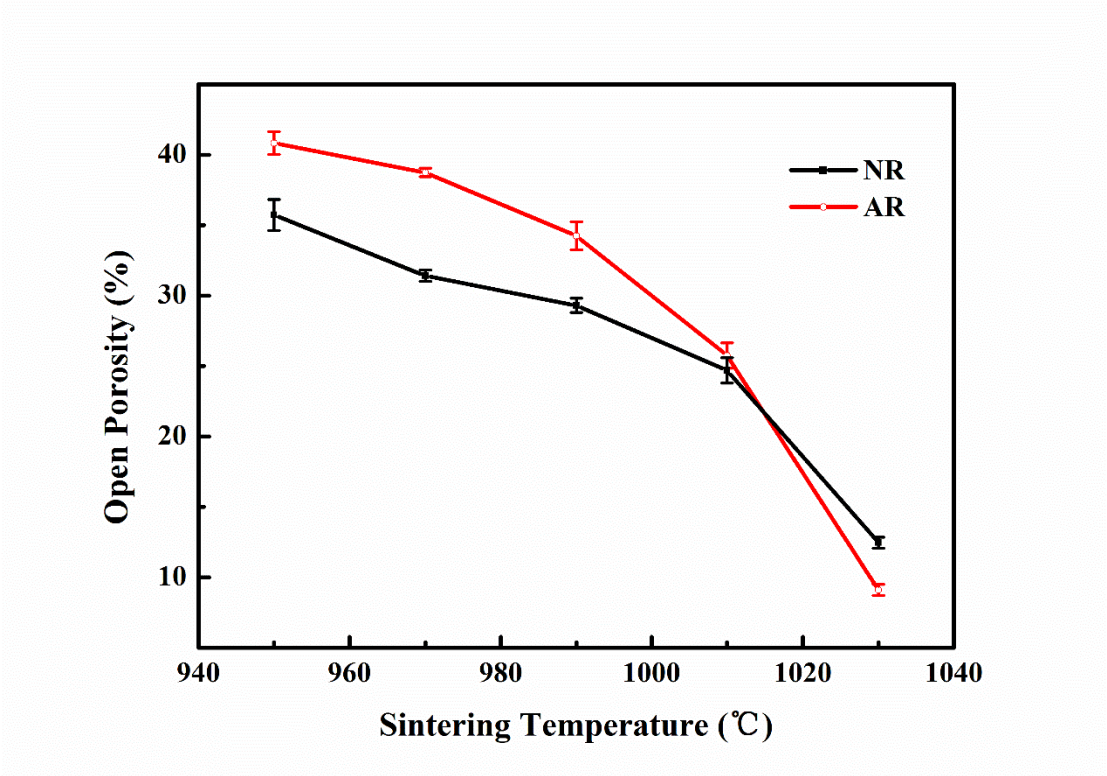

Fig. 5 Open porosity of the sintered samples from two kinds of powders.

3.4. Grain Development in Sintering Procedure

For better understanding the grain morphology in ceramics NR1030 and AR1030, and better inference the grain growth mechanism, the surface of as-sintered samples was etched by HF solution (as shown in Fig. 6). Rod-shaped $Li_2Si_2O_5$ grains were observed in both NR1030 an AR1030. Like what were discussed in Fig. 4, more uniform grain morphology was detected on the surface of AR1030. Two reasons might result in the large grains in NR1030. One was the aggregated particles, the other was the existence of second phase[32].

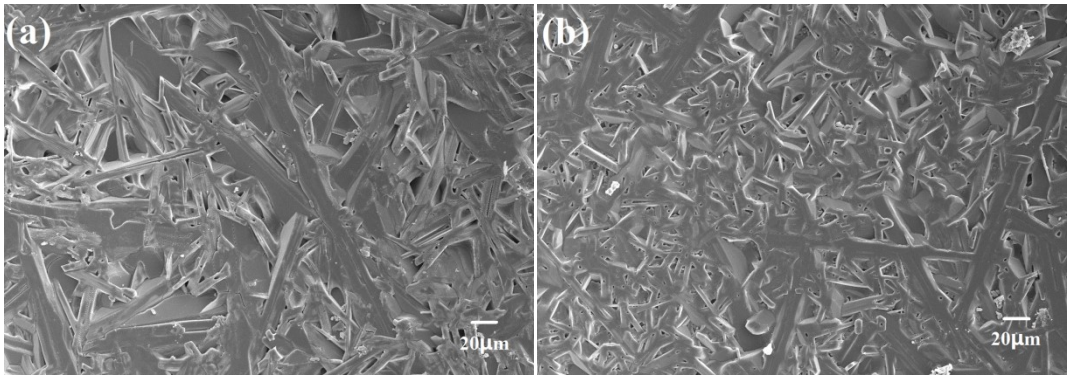

Fig. 6 SEM micrographs of the etched surface from sintered samples: (a) NR1030; (b) AR1030.

Crystallization and grain growth procedure of $Li_2Si_2O_5$ grains during sintering was illustrated in Fig. 7. As shown in Fig. 7(a), in the melted-glass based method (both in the melting-casting-

crystallization method and in the sintering of glass frits method), nucleation regions generated at first either by compositional and energetic fluctuations or by phase separation. Nuclei would emerge in the nucleation regions when nucleation agent was added. Then Li_2SiO_3 and $Li_2Si_2O_5$ grains nucleated and grew from these regions. Morphology of $Li_2Si_2O_5$ grains could be controlled by nucleation agent in this method[20]. In the reaction method, $Li_2Si_2O_5$ grains developed from another way in Fig. 7(b). During the sintering procedure, $Li_2Si_2O_5$ nuclei generated at the boundaries of Li_2SiO_3 and SiO_2 grains firstly. Then $Li_2Si_2O_5$ grains grew from these sites along with the consumption of Li_2SiO_3 and SiO_2, and developed into rod-like grains[26]. The $Li_2Si_2O_5$ possessed orthorhombic structure (a=5.683, b=4.784, c=14.648Å), because the $Li_2Si_2O_5$ crystals grew along the c-axis was faster and more stable, $Li_2Si_2O_5$ grains always grew into rod-like. Additionally, the lattice parameter *c* started to increase with temperature higher than 780°C, which also promoted the anisotropic growth of $Li_2Si_2O_5$ grains into elongated morphology[27]. In the sintering of sol-gel derived $Li_2Si_2O_5$ powders, grain morphology was developed in different way from what were mentioned above. No external nuclei from nucleation agent or internal $Li_2Si_2O_5$ nuclei through reaction were generated in this sintering procedure. Since $Li_2Si_2O_5$ crystals were fabricated through heat treatment, sintering process was controlled by the growth of $Li_2Si_2O_5$ grains. At the beginning of sintering, big $Li_2Si_2O_5$ grains grew up and small $Li_2Si_2O_5$ grains disappeared. No specific directionality emerged in grain growth, thus grains grew simultaneously in all directions. Thus, $Li_2Si_2O_5$grains developed into large equiaxial grains at first, and then grew into rod-shaped grains. As shown in Fig. 7(c), $Li_2Si_2O_5$ grains obtained through this mechanism were larger than the other two models. In the sintering of sol-gel derived $Li_2Si_2O_5$ powders, no extra nucleation agents or other additions were needed. Thus, $Li_2Si_2O_5$ glass-ceramics fabricated through this method only contained slight glass phases.

Since the sources of lithium and silicon were mixed with a stoichiometric molar ration of 1/1, and no extra additives were added, which resulted in less amount of glass phases in sol-gel derived $Li_2Si_2O_5$ glass-ceramics compared to those prepared by melting methods. For sol-gel derived glass-ceramics, $Li_2Si_2O_5$ crystals already formed in the calcination procedure and then grew into rod-shaped crystals during the sintering procedure. While, for the case of melting prepared glass-ceramics, $Li_2Si_2O_5$ crystals precipitated from the glass matrix and then grew into rod-shaped crystals during the crystallization procedure. That is to say, the sintering characteristic of sol-gel derived $Li_2Si_2O_5$ glass-ceramics is more like that of ceramics.

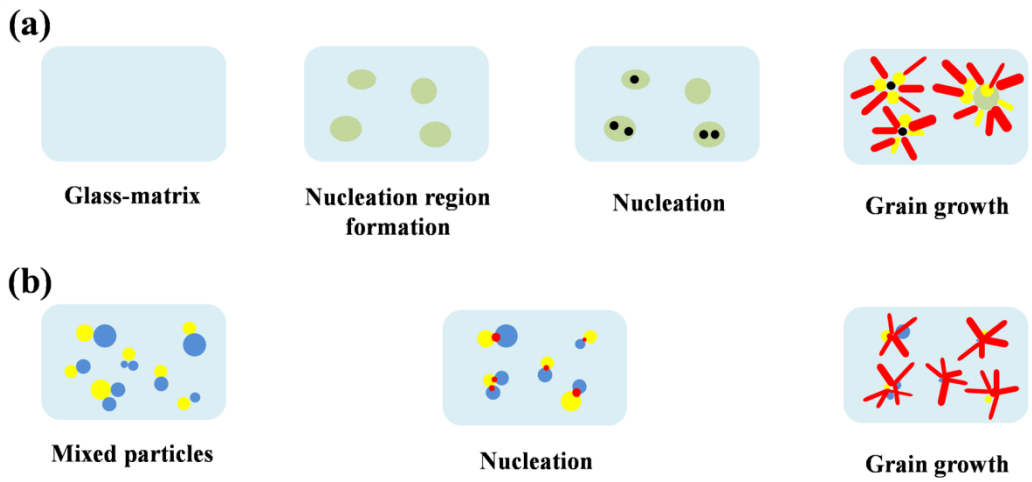

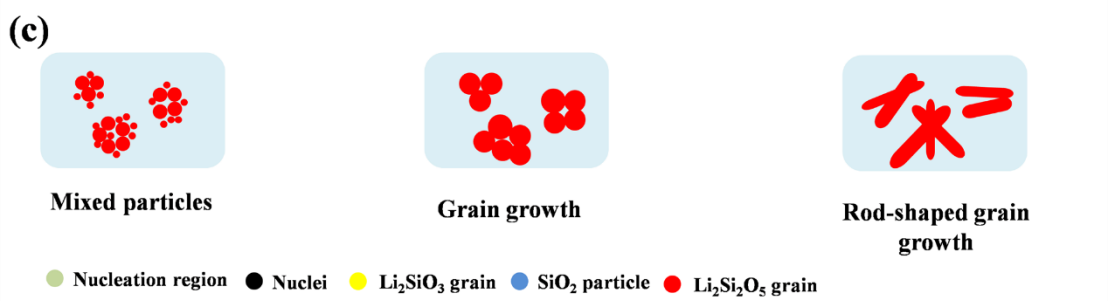

Fig. 7 Crystallization and grain growth models in the sintering of $Li_2Si_2O_5$ glass-ceramics: (a) melted-glass based method; (b) reaction sintering method; (c) $Li_2Si_2O_5$ powders from sol-gel method.

4. Conclusion

In the present work, lithium disilicate ($Li_2Si_2O_5$) glass-ceramics were fabricated by nitrate route and alkoxide route. Single-phase $Li_2Si_2O_5$ glass-ceramics was obtained through alkoxide route. On the contrary, the powders prepared by nitrate route contained small amount of Li_2SiO_3. $Li_2Si_2O_5$ powders prepared by alkoxide route were much more homogenous than the powders prepared by nitrate route, and the former had a much smaller particle size. Accordingly, samples sintered from alkoxide-derived powders had smaller grain size and more uniform microstructure. With the increase of sintering temperature, the grain size in both samples increased, while the open porosity decreased as expected. The $Li_2Si_2O_5$ grains were near-equiaxed at the early stage of sintering, and then transformed into rod-shaped grains at higher sintering temperature. The sintering characteristic of sol-gel derived $Li_2Si_2O_5$ glass-ceramics is more like that of ceramics.

Acknowledgments

The work was financially supported by Shanghai Committee of Science and Technology, China (17441904100).

Compliance with ethical standards

Conflict of interest The authors declare that they have no conflict of interest.

References

[1] M. Kern, H. Knode, J.R. Strubb, The all-porcelain, resin-bonded bridge, Quintessence International, 22 (1991) 257.

[2] M. Andersson, A. Odén, A new all-ceramic crown: A dense-sintered, high-purity alumina coping with porcelain, Acta Odontologica Scandinavica, 51 (1993) 59-64.

[3] J. Tinschert, G. Natt, W. Mautsch, M. Augthun, H. Spiekermann, Fracture resistance of lithium disilicate-, alumina-, and zirconia-based three-unit fixed partial dentures: a laboratory study, International Journal of Prosthodontics, 14 (2001) 231.

[4] A. Sundh, M. Molin, G. Sjögren, Fracture resistance of yttrium oxide partially-stabilized zirconia all-ceramic bridges after veneering and mechanical fatigue testing, Dental Materials Official Publication of the Academy of Dental Materials, 21 (2005) 476-482.

[5] N.J. Grey, V. Piddock, M.A. Wilson, In vitro comparison of conventional crowns and a new all-ceramic system, Journal of Dentistry, 21 (1993) 47-51.

[6] A. Aldegheishem, G. Ioannidis, W. Att, H. Petridis, Success and Survival of Various Types of All-Ceramic Single Crowns: A Critical Review and Analysis of Studies with a Mean Follow-Up of 5 Years or Longer, International Journal of Prosthodontics, 30 (2017) 168.

[7] J. Conejo, R. Nueesch, M. Vonderheide, M.B. Blatz, Clinical Performance of All-Ceramic Dental Restorations, Current Oral Health Reports, (2017) 1-12.

[8] W. Holand, G.H. Beall, Glass Ceramic Technology, (2012).

[9] J.B. Quinn, V. Sundar, I.K. Lloyd, Influence of microstructure and chemistry on the fracture toughness of dental ceramics, Dental Materials, 19 (2003) 603.

[10] R.G. Ritter, Multifunctional uses of a novel ceramic-lithium disilicate, Journal of Esthetic & Restorative Dentistry, 22 (2010) 332-341.

[11] M.J. Heffernan, S.A. Aquilino, A.M. Diaz-Arnold, D.R. Haselton, C.M. Stanford, M.A. Vargas, Relative translucency of six all-ceramic systems. Part II: core and veneer materials, Journal of Prosthetic Dentistry, 88 (2002) 10-15.

[12] M.J. Heffernan, S.A. Aquilino, A.M. Diaz Arnold, D.R. Haselton, C.M. Stanford, M.A. Vargas, Relative translucency of six all-ceramic systems. Part I: Core materials, Journal of Prosthetic Dentistry, 88 (2002) 4-9.

[13] W. Höland, V. Rheinberger, E. Apel, t.H.C. Van, M. Höland, A. Dommann, M. Obrecht, C. Mauth, U. Graf-Hausner, Clinical applications of glass-ceramics in dentistry, Journal of Materials Science: Materials in Medicine, 17 (2006) 1037-1042.

[14] G.G. Boiko, G.A. Sycheva, L.G. Valjuk, Influence of Synthesis Conditions on the Kinetics of Crystallization of Photosensitive Lithium Silicate Glasses, Glass Physics and Chemistry, 21 (1995) 45-52.

[15] Sycheva G.A. Sol–Gel Synthesis of Photostructured Gold_Containing Lithium Silicate Glasses, Glass Physics and Chemistry, 37 (2011) 495–503.

[16] Sycheva G.A., Kostyreva T.G. Nucleation and Morphology of Crystals in Simple and Complex Silicate Glasses R'2O-SiO2, R'2O-R"O-SiO2, (R' = Li, Na, K; R" = Ca, Mg) Synthesized by the Sol-Gel Method 40 (2014) 513–520.

[17] T.B. Zhang, A.J. Easteal, N.R. Edmonds, B. Debes, Sol–Gel Preparation and Characterization of Lithium Disilicate Glass–Ceramic, Journal of the American Ceramic Society, 90 (2007) 1592-1596.

[18] P. Li, L.F. Francis, Sol-gel processing of lithium disilicate, Journal of Materials Science, 30 (1995) 6192-6204.

[19] P.C.S. Jr, E.D. Zanotto, V.M. Fokin, H. Jain, TEM and XRD study of early crystallization of lithium disilicate glasses, Journal of Non-Crystalline Solids, 331 (2003) 217-227.

[20] X. Zheng, G. Wen, L. Song, X.X. Huang, Effects of P_2O_5 and heat treatment on crystallization and microstructure in lithium disilicate glass ceramics, Acta Materialia, 56 (2008) 549-558.

[21] S. Huang, P. Cao, C. Wang, Z. Huang, W. Gao, Fabrication of a high-strength lithium disilicate glass-ceramic in a complex glass system, Journal of Asian Ceramic Societies, 1 (2013) 46–52.

[22] K. Yuan, F. Wang, J. Gao, X. Sun, Z. Deng, H. Wang, J. Chen, Effect of sintering time on the microstructure, flexural strength and translucency of lithium disilicate glass-ceramics, Journal of Non-Crystalline Solids, 362 (2013) 7-13.

[23] G. Wen, X. Zheng, L. Song, Effects of P_2O_5 and sintering temperature on microstructure and mechanical properties of lithium disilicate glass-ceramics, Acta Materialia, 55 (2007) 3583-3591.

[24] T. Zhao, Y. Qin, B. Wang, J.F. Yang, Improved densification and properties of pressureless-sintered lithium disilicate glass-ceramics, Materials Science & Engineering A, 620 (2015) 399-406.

[25] H.R. Fernandes, D.U. Tulyaganov, M.J. Pascual, V.V. Kharton, A.A. Yaremchenko, J.M.F. Ferreira, The role of K_2O on sintering and crystallization of glass powder compacts in the $Li_2O–K_2O–Al_2O_3–SiO_2$ system, Journal of the European Ceramic Society, 32 (2012) 2283-2292.

[26] T. Zhao, Y. Qin, P. Zhang, B. Wang, J.F. Yang, High-performance, reaction sintered lithium disilicate glass–ceramics, Ceramics International, 40 (2014) 12449-12457.

[27] Huang S, Huang Z, Gao W, et al. In Situ High-Temperature Crystallographic Evolution of a Nonstoichiometric Li2O· 2SiO2 Glass. Inorganic chemistry, 52(2013) 14188-14195.

[28] N. Karpukhina, H.A. Abomosallam, R.G. Hill, R.V. Law, Effect of sodium, potassium and zinc substitutions in lithium disilicate glass and glass-ceramics, Physics & Chemistry of Glasses, volume 54 (2013) 76-83(78).

[29] S.H. Knickerbocker, A.H. Kumar, L.W. Herron, Cordierite glass-ceramics for multilayer ceramic packaging, American Ceramic Society Bulletin, 72 (1993) 90-95.

[30] H.R. Fernandes, D.U. Tulyaganov, I.K. Goel, J.M.F.F., Crystallization Process and Some Properties of $Li_2O–SiO_2$Glass–Ceramics Doped with Al_2O_3 and K_2O, Journal of the American Ceramic Society, 91 (2008) 3698–3703.

[31] P. Li, B.A. Ferguson, L.F. Francis, Sol–Gel Processing Lithium Disilicate. Part I. Crystalline Phase Development of Gel-Derived Powders, Journal of Materials Science, 30 (1995) 4076-4086.

[32] Lupulescu A, Glicksman ME. Diffusion-limited crystal growth in silicate systems: similarity with high-pressure liquid-phase sintering. Journal of Crystal Growth. 211(2000) 49-61.